

Spinon excitation spectra of the J_1 - J_2 chain from analytical calculations in the dimer basis and exact diagonalization

Arthur Lavarélo and Guillaume Roux

LPTMS, Univ. Paris-Sud and CNRS, UMR 8626, F-91405 Orsay, France.

October 29, 2014

Abstract. The excitation spectrum of the frustrated spin-1/2 Heisenberg chain is reexamined using variational and exact diagonalization calculations. We show that the overlap matrix of the short-range resonating valence bond states basis can be inverted which yields tractable equations for single and two spinons excitations. Older results are recovered and new ones, such as the bond-state dispersion relation and its size with momentum at the Majumdar-Ghosh point are found. In particular, this approach yields a gap opening at $J_2 = 0.25J_1$ and an onset of incommensurability in the dispersion relation at $J_2 = 9/17J_1$ [as in S. Brehmer *et al.*, J. Phys.: Condens. Matter **10**, 1103 (1998)]. These analytical results provide a good support for the understanding of exact diagonalization spectra, assuming an independent spinons picture.

PACS. 75.10.Jm Quantized spin models, including quantum spin frustration – 75.10.Kt Quantum spin liquids, valence bond phases and related phenomena – 75.50.Pq Spin chain models – 75.40.Mg Numerical simulation studies

Frustration in antiferromagnetic magnets is one of the key ingredient to stabilize exotic phases [1]. In one-dimension, where quantum fluctuations destroy the Néel order, a next-nearest neighbor coupling is known to bring two main features. There is first a transition from the quasi-long range ordered phase to a gapped phase which order parameter is the dimerization, breaking translational invariance. The second is the onset of incommensurability in the spin correlations and dispersion relation of elementary excitations. The J_1 - J_2 frustrated chain model is thus a paradigmatic model for quantum magnetism which has been widely studied and from which stemmed the physics of valence bond solid phases.

We start by recalling known results on the frustrated spin-1/2 chain Hamiltonian which reads

$$\mathcal{H} = \sum_{i=1}^L J_1 \mathbf{S}_i \cdot \mathbf{S}_{i+1} + J_2 \mathbf{S}_i \cdot \mathbf{S}_{i+2}, \quad (1)$$

in which $J_{1,2} > 0$ are antiferromagnetic couplings and \mathbf{S}_i are spin-1/2 operators. L denotes the length of the chain and periodic or open boundary conditions can be used.

The phase transition to a dimerized state can be understood by bosonization arguments, leading to a Kosterlitz-Thouless type of transition [2,3,4]. The transition point can be efficiently determined by level spectroscopy [5] and is found to be located at $J_2/J_1 \simeq 0.241167$ [3,5,6]. One peculiarity of the transition is the disappearance of logarithmic corrections associated with $SU(2)$ symmetry right at the critical point [6]. Another way to understand the opening of the gap and the onset of a dimerized phase

is to start the bosonization from the limit of two chains coupled in a zig-zag geometry [7], ie. the $J_2 \gg J_1$ limit. Then, the gap is shown to decay exponentially with J_2/J_1 , so as the dimerization. Between both regimes, the gap and dimerization curves display a intermediate maximum (not at the same location for both quantity) which is captured by numerics [3,7]. Deep in the dimerized phase, the two degenerate ground-states in the thermodynamical limit are well pictured by the Majumdar-Ghosh (MG) state which is a product of decoupled dimers on bonds $|\text{MG}\rangle = |\cdots \bullet\bullet \bullet\bullet \bullet\bullet \bullet\bullet \bullet\bullet \cdots\rangle$, where dimers are represented by $|\bullet\bullet\rangle = \frac{1}{\sqrt{2}}(|\uparrow\downarrow\rangle - |\downarrow\uparrow\rangle)$ and an even length is assumed. Actually, for the special value $J_2 = J_1/2$, this MG state is the exact ground-state of the Hamiltonian [8, 9]. Similar and generalization of such valence bond solid states have been found in other models and remain an active field of research since having exact and simple ground-states to non-trivial Hamiltonians is essential to the understanding of quantum magnetism.

The other feature introduced by frustration is incommensurability in real-space spin correlations: they start to oscillate at a wave-vector $q \neq \pi$ above a point called the disorder point. This effect already emerges in the classical limit [10] in which it is simply understood as a best compromise between the two couplings, one aiming to order at π while the other aims to order at $\pi/2$. The classical disorder point is at $J_2/J_1 = 0.25$. In the quantum version, the easiest, and actually the only quantitative way so far, is to compute numerically the real-space spin correlations [3,7,11,12]. It can be argued [13] that the onset of incommensurability should match the minimum of

the spin correlation length which corresponds to the MG point in the model under study. This scenario is confirmed in the numerics and also supported by variational [14] and perturbative [15] arguments. Moreover, incommensurability will naturally show up in the spin structure factor then [7,14,16]. Yet, in the presence of a finite correlation length, the onset of incommensurability in this signal occurs for a stronger frustration [13], called the Lifshitz point. This point has been estimated numerically at $J_2/J_1 = 0.52036$ [16], and it has been recently shown that for odd chains (in which the MG state cannot be the ground-state), the Lifshitz point is actually shifted toward a larger value $J_2/J_1 = 0.538$.

Last, the dispersion relation becomes incommensurate too, in the sense that the minimum of the triplet excitation lies at a wave-vector away from the $K = \pi$ antiferromagnetic wave-vector, and for which we will use the notation q^* in the following. The connection between dispersion relation and spin correlations is not physically straightforward. Still, approximations such as the single-mode approximation help capture the minimum of the dispersion relation from correlators [15,17]. This approach works best for gapped systems and was successfully applied to other models known to display incommensurability, such as the spin one bilinear-biquadratic chain [18,19]. In the situation of two strongly coupled J_1 - J_2 chains, one can even analytically show that $q^* \neq q$ [20]. Together with the dispersion relation, the dynamics of elementary excitations has been investigated in several limits of the model. For the Heisenberg chain, the Bethe-ansatz solution provides a quantitative and physically transparent picture in terms of two-spinons continuum, corresponding to the so-called des-Cloizeaux Pearson law [21,22,23]. Multi-spinons or multi-magnons contributions have recently been shown to be relevant in the spectral weight of several dynamical structure factors [24,25,26]. At the MG point, variational methods have been used to tackle the dispersion relation [27,28,29,30,31,32,33,34,35]. Working in the dimer basis gave a good account for the shape of the dispersion relation, with in particular the explanation for a triplet bound-state [27] close to $K = \pi/2$. Going away from the MG point is more difficult and other techniques such as matrix-product states [36] have been used to clarify the behavior and the onset of incommensurability that was found to be at $J_2/J_1 = 9/17 \simeq 0.52941$. This shows that this defines a third different point for the onset of incommensurability.

In addition to the spontaneously dimerized phase, an explicit alternating nearest neighbor coupling $J_1 + (-1)^i \delta$ will explicitly break translational invariance and bring the system into the spin-Peierls phase [37]. The MG point condition can be generalized in this case and a non-zero δ -term induces the confinement of spinon excitations [38,39,40,41]. Many works have been devoted to this physics, using numerical and analytical methods [30,31,37,39,42,41,43,44,45,46,47] to characterize the confinement between two spinons, leading to a bound-state, as well as the confinement to a chain end for odd length systems.

In this paper, we study the elementary spinon excitations of the J_1 - J_2 chain using a variational description well suited for the MG point and extending the results around it to capture features such as the dimerization transition and the onset of incommensurability. The variational method in the resonating valence bond (RVB) basis has already been used previously [27,28,30,31,34,35] and we show that more analytical results can be obtained by a systematic projection of the Hamiltonian on this basis, rather than solving numerically the generalized eigenvalue problem, as usually done. This strategy was first used successfully in the case of a random MG chain [48]. To complete this approach on elementary excitations, the results are compared to exact diagonalization (ED) spectra showing a good description of both single and many spinons excitations.

The paper is organized as follows: we first present the RVB variational approach and the way one can derive an effective Hamiltonian from it. The method is then applied to the single spinon dispersion relation at, and away from the MG point. We then move to the two-spinon spectrum which is obtained only for the MG point but with an explicit determination of the triplet bound-state size. Comparison of ED with an independent spinons ansatz is given. Last, we discuss the situation of explicit dimerization, deriving properly the confinement of a single spinon and showing how to obtain the two-spinon excitation spectrum analytically at the MG point.

1 The RVB basis variational method

1.1 Presentation of the method in the case of a single spinon excitation

In order to study the dynamics of a single spinon, one can work on an odd size chain of length L . We assume open boundary conditions, so that the spinon lives on one of the two sub-lattice only. Using periodic boundary conditions would make the spinon jump on the other sub-lattice while arriving at the end of the chain, corresponding to a doubling of the number of available sites (roughly doubling the system size). The variational approach consists in working with the subspace generated by states of the form $|2i\rangle = |\cdots \bullet \cdots \uparrow \cdots \bullet \cdots\rangle$ with a spinon at site $2i$ ($i \in [0, \frac{L-1}{2}]$) which separates two MG domains. These states are clearly intuitive for the MG point. They constitute a free family but they do not span [49] the whole spin sector $\{S_{\text{tot}} = 1/2, S_{\text{tot}}^z = 1/2\}$, making the approach variational. Notice that including the spinon states living on the other sublattice, as one would do with periodic boundary conditions, makes the family over-complete and we thus prefer to work with open boundary conditions. A crucial point is that the states are non-orthogonal. The overlap matrix $[\mathcal{O}]$ (in the following, we use the notation $[A]$ for the matrix representation of operator A since Dirac notation can be confusing while working with non-

orthogonal states) has elements

$$[\mathcal{O}]_{ij} = \langle 2i|2j \rangle = \left(-\frac{1}{2}\right)^{|i-j|}. \quad (2)$$

1.2 Effective Hamiltonian

The goal of the variational approach is to diagonalize the restriction $\tilde{\mathcal{H}}$ of \mathcal{H} in the subspace $\{|2i\rangle\}$ for which we have

$$\tilde{\mathcal{H}} = P\mathcal{H}P, \quad (3)$$

where P is the orthogonal projector on that subspace. Since P is self-adjoint, the effective Hamiltonian $\tilde{\mathcal{H}}$ is self-adjoint two which ensures that its eigenvalues are real. Diagonalizing the representation of $\tilde{\mathcal{H}}$ in the basis $\{|2i\rangle\}$ is a generalized eigenvalue problem that reads

$$\sum_i \langle 2j|\mathcal{H}|2i\rangle \psi_i = E \sum_i \langle 2j|2i\rangle \psi_i. \quad (4)$$

where E is an eigenenergy and

$$|\psi\rangle = \sum_i \psi_i |2i\rangle \quad (5)$$

is the decomposition of the associated eigenfunction in this basis.

We would like to stress the fact that the $\langle 2j|\tilde{\mathcal{H}}|2i\rangle$ are not the matrix elements $[\tilde{\mathcal{H}}]_{ij}$ of $\tilde{\mathcal{H}}$ in the basis $\{|2i\rangle\}$ since the latter is non-orthogonal. Yet, they are connected by the projector P which writes as the inverse of the overlap matrix

$$P = \sum_{ij} [\mathcal{O}^{-1}]_{ij} |2i\rangle \langle 2j|. \quad (6)$$

Then, one gets the relation

$$[\tilde{\mathcal{H}}]_{ij} = \sum_k [\mathcal{O}^{-1}]_{ik} \langle 2k|\mathcal{H}|2j\rangle. \quad (7)$$

In general, inverting the overlap matrix is hard and authors prefer to solve (4) directly with numerical methods. However, in the case of a chain, we found that the inverse of the overlap matrix takes the following tridiagonal form

$$[\mathcal{O}^{-1}] = \frac{1}{3} \begin{pmatrix} 4 & 2 & & & \\ 2 & 5 & 2 & & \\ & 2 & 5 & 2 & \\ & & \ddots & \ddots & \ddots \\ & & & 2 & 5 & 2 \\ & & & & 2 & 4 \end{pmatrix}, \quad (8)$$

which will allow some analytical solutions of the diagonalization of the effective Hamiltonian.

Notice that we do not specify any particular Hamiltonian so far and the approach could be used to spin-1/2

chain models other than the frustrated chain. In what follows, we work with (1) which can be rewritten at the MG point as

$$\mathcal{H}_{\text{MG}} = J \sum_i (2\mathbf{S}_i \cdot \mathbf{S}_{i+1} + \mathbf{S}_i \cdot \mathbf{S}_{i+2}), \quad (9)$$

with $J = J_2$. We also recall two basic facts on the two MG states. Their energy is

$$E_{\text{MG}} = -\frac{3}{4}LJ, \quad (10)$$

for periodic boundary conditions and for the ground-state with open boundary conditions. Second, they are non-orthogonal and their overlap reads

$$\langle \text{MG}|\text{MG}' \rangle = -\left(-\frac{1}{2}\right)^{\frac{L}{2}-1}, \quad (11)$$

irrespective of the boundary conditions.

2 Dynamics of a single spinon

2.1 Dispersion relation at the MG point

We first show how the method allows one to recover the spinon dispersion relation at the MG point. To do so, we look at the application of the terms in (9) on a basis state $|2j\rangle = |\cdots \bullet \bullet \bullet \uparrow \bullet \bullet \bullet \cdots\rangle$:

$$\mathbf{S}_{2j} \cdot \mathbf{S}_{2j+1} |2j\rangle = +\frac{1}{4} |2j\rangle + \frac{1}{2} |\cdots \bullet \bullet \bullet \uparrow \bullet \bullet \bullet \cdots\rangle, \quad (12)$$

$$\mathbf{S}_{2j} \cdot \mathbf{S}_{2j+2} |2j\rangle = -\frac{1}{4} |2j\rangle - \frac{1}{2} |\cdots \bullet \bullet \bullet \uparrow \bullet \bullet \bullet \cdots\rangle, \quad (13)$$

$$\mathbf{S}_{2j-1} \cdot \mathbf{S}_{2j+1} |2j\rangle = +\frac{1}{4} |2j\rangle + \frac{1}{2} |\cdots \bullet \bullet \bullet \uparrow \bullet \bullet \bullet \cdots\rangle. \quad (14)$$

One can check that the last state (14) is orthogonal to the variational subspace. Then, we deduce the restriction of \mathcal{H}_{MG} to this subspace

$$(\tilde{\mathcal{H}}_{\text{MG}} - E_{\text{MG}}) |2j\rangle = \frac{J}{2} \left(|2j-2\rangle + \frac{5}{2} |2j\rangle + |2j+2\rangle \right), \quad (15)$$

where E_{MG} is given by (10) extrapolated to odd sizes. Thus, we are left with a simple tight-binding Hamiltonian which is straightforwardly diagonalized by Fourier transformation of the states

$$|k\rangle = \sum_j e^{ik2j} |2j\rangle, \quad (16)$$

with $k \in [\frac{\pi}{2}, \frac{\pi}{2}]$ due to the folding of the Brillouin zone. Then, the well-known [27] dispersion relation of a single spinon at the MG point is recovered

$$\omega(k) = J \left(\frac{5}{4} + \cos 2k \right). \quad (17)$$

2.2 Away from the MG point: single spinon gap and incommensurability

We now show that the same approach can be extended away from the MG point, capturing the main two features of the phase diagram: the transition to a gapless phase at small J_2 and the onset of incommensurability in the dispersion relation. This is done by rewriting (1) as

$$\mathcal{H} = \mathcal{H}_{\text{MG}} + \eta \sum_i \mathbf{S}_i \cdot \mathbf{S}_{i+1}, \quad (18)$$

with the parametrization $\eta = J_1 - 2J$ which measures the distance from the MG point. The η -term is simply a nearest-neighbor term which, when applied to state $|2j\rangle$, generates diagonal terms and, more importantly, terms with dimer excitations of the form

$$\begin{aligned} \mathbf{S}_{2i-1} \cdot \mathbf{S}_{2i} |2j\rangle &= \frac{1}{4} |2j\rangle + \frac{1}{2} |[2i-2, 2i+1], 2j\rangle \quad (i < j), \\ \mathbf{S}_{2i} \cdot \mathbf{S}_{2i+1} |2j\rangle &= \frac{1}{4} |2j\rangle + \frac{1}{2} |2j, [2i-1, 2i+2]\rangle \quad (i > j), \end{aligned}$$

in which $|[2i-2, 2i+1], 2j\rangle = |\dots \overbrace{\bullet \bullet}^{\text{dimer}} \dots \uparrow \bullet \dots\rangle$ is the state having a spinon at site $2j$ and a singlet between sites $2i-2$ and $2i+1$. The overlaps of these states with $|2j\rangle$ match

$$\begin{aligned} \langle 2j | [2n-2, 2n+1], 2i \rangle &= -\frac{1}{2} \langle 2j | 2i \rangle (1 + 3\Theta(n-j-1)), \\ \langle 2j | 2i, [2n-1, 2n+2] \rangle &= -\frac{1}{2} \langle 2j | 2i \rangle (1 + 3\Theta(j-n-1)), \end{aligned}$$

with Θ the Heaviside function such that $\Theta(0) = 1$. One then obtains the projection onto the variational subspace as

$$\begin{aligned} P|[2n-2, 2n+1], 2i\rangle &= -\frac{1}{2} |2i\rangle - \left(-\frac{1}{2}\right)^{i-n+1} |2n\rangle \\ &\quad + \left(-\frac{1}{2}\right)^{i-n} |2n-2\rangle, \\ P|2i, [2n-1, 2n+2]\rangle &= -\frac{1}{2} |2i\rangle - \left(-\frac{1}{2}\right)^{n-i+1} |2n\rangle \\ &\quad + \left(-\frac{1}{2}\right)^{n-i} |2n+2\rangle. \end{aligned}$$

Thus, the correction to the MG Hamiltonian creates arbitrary long hoppings of dimers which amplitude decreases exponentially with distance. Finally, the effective Hamiltonian is a full matrix for which we have

$$\begin{aligned} (\tilde{\mathcal{H}} - E_0) |2j\rangle &= \left(\frac{5}{4}J + \frac{7}{8}\eta\right) |2j\rangle \\ &\quad + \frac{1}{2}(J + \eta) (|2j-2\rangle + |2j+2\rangle) \\ &\quad + \eta \sum_{n < j} \left(-\frac{1}{2}\right)^{j-n} \left(\frac{1}{4} |2n\rangle + \frac{1}{2} |2n-2\rangle\right) \\ &\quad + \eta \sum_{n > j} \left(-\frac{1}{2}\right)^{n-j} \left(\frac{1}{4} |2n\rangle + \frac{1}{2} |2n+2\rangle\right), \end{aligned} \quad (19)$$

where we define $E_0 = E_{\text{MG}} - \frac{3}{8}\eta L$ as the origin of energies. Fourier transforming this relation gives the dispersion relation

$$\begin{aligned} \omega(k) &= \frac{5}{4}J + \frac{7}{8}\eta + (J + \eta) \cos(2k) \\ &\quad + \frac{\eta}{2} \sum_{n>0} \left(-\frac{1}{2}\right)^n (\cos(2kn) + 2\cos[2k(n+1)]) . \end{aligned} \quad (20)$$

The summation can be carried out, leading to the following compact form

$$\begin{aligned} \omega(k) &= \frac{7}{8}J_1 - \frac{1}{2}J_2 + (J_1 - J_2) \cos 2k \\ &\quad + 4(J_1 - 2J_2) \frac{\sin^2 2k}{5 + 4 \cos 2k}. \end{aligned} \quad (21)$$

The same dispersion relation, though written differently and with a different constant, was obtained from a matrix-product states ansatz in Ref. [36]. Their gap was not the same because the constant factor is different. Within our variational approach, we obtain a vanishing gap for $J_2 = 0.25J_1$ which is actually rather close to the numerical value for the transition, thereby giving a simple picture for the onset of the transition, starting from the dimerized phase. We will come back to this point in Section 3.

The minimum of the dispersion relation is at $k = \pi/2$ for small J_2 but becomes incommensurate above the threshold $J_2/J_1 = 9/17 \simeq 0.52941$. This value is the same as in Ref. [36] and in agreement with the recent numerical study of Ref. [35]. In the incommensurate regime, the position k^* of the minimum of the single-spinon dispersion relation follows

$$k^* = \frac{1}{2} \arccos \left(-\frac{5}{4} + \frac{3}{4} \sqrt{2 - \frac{J_1}{J_2}} \right). \quad (22)$$

Close to the threshold, the wave-vector thus displays a discontinuity in its derivative with an exponent $1/2$ in the distance from commensurability:

$$\frac{\pi}{2} - k^* \propto \left(\frac{J_2}{J_1} - \frac{9}{17} \right)^{1/2}. \quad (23)$$

A similar square-root behavior was obtained in the frustrated ladder case [20] and is compatible with the generic scenario for the onset of incommensurability [13].

2.3 Evolution of the dispersion relation with frustration

With these results, we can sketch the overall behavior of the single spinon dispersion relation with increasing frustration. Exact diagonalization spectra have been computed using the Lanczos algorithm on a symmetrized Hilbert space in both the $S_{\text{tot}}^z = 1/2$ and $S_{\text{tot}}^z = 3/2$ sectors to observe the opening of the gap and the onset of incommensurability. The single spinon spectrum at the MG point was given in Ref. [39]. The results are displayed

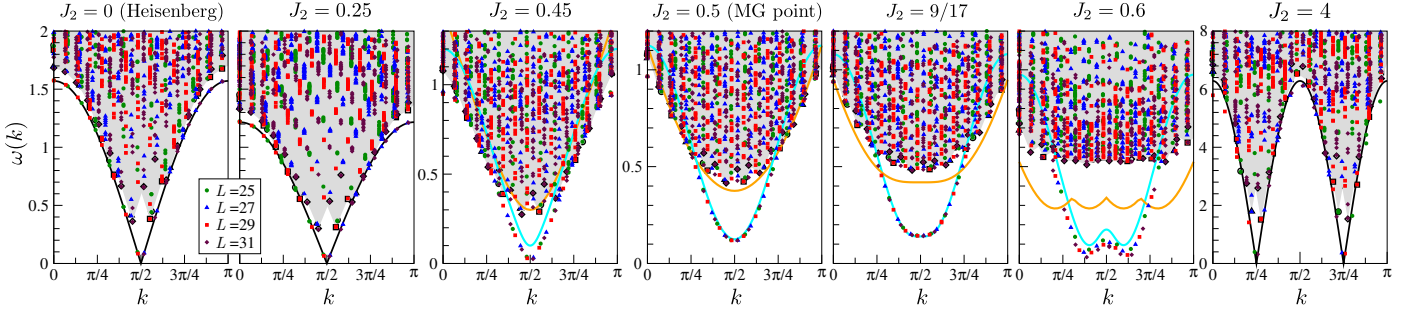


Fig. 1. Single spinon dispersion relations: variational predictions are plotted against exact diagonalization data on odd size chains for increasing frustration J_2 , taking $J_1 = 1$ as the unit of energy. The grey area represents the region for which energies belong to the $S^z_{\text{tot}} = 3/2$ sector in ED. The black curves are the lowest branches of spinon dispersion expected from Bethe ansatz calculations. For $J_2 = 0$, the $J_1 \frac{\pi}{2} |\cos k|$ is exact while for $J_2 = 0.25J_1$, the prefactor is fitted to the curve. In the $J_2 = 4J_1$ plot, $J_2 \frac{\pi}{2} |\cos 2k|$ is used as the system consists in almost decoupled chains with double lattice spacing. Notice that, strictly speaking, plots with $J_2 = 0.25J_1$ and $J_2 = 4J_1$ correspond to gapped systems but the gap is so small that the ED data cannot resolve it and the Bethe ansatz curve reproduce well the higher energies part. The cyan curve is the variational result (21). The orange curve is the lowest branch of 3-spinons dispersion relation in the variational approach and assuming independent spinons, to be compared to the region of states with $S^z_{\text{tot}} = 3/2$.

on Fig. 1 for seven typical values of J_2/J_1 . First, we recall the physics of the Heisenberg point ($J_2 = 0$) which is exactly solvable by Bethe ansatz and for which the lowest spinon branch reads $\omega(k) \simeq J_1 \frac{\pi}{2} |\cos k|$ (black curve). For $J_2 = 0.25J_1$, finite-size effects prevent ED from a clear determination of the tiny gap that exists in the thermodynamical limit, and we observe that the higher energies of the lowest spinon are well reproduced by the Bethe ansatz (or spin-wave) form with a prefactor smaller than $\pi/2$. In both cases, the three-spinons energies collapse on the single spinon energy.

Entering deep in the dimerized phase for $J_2 = 0.45J_1$, we observe the finite gap in the dispersion relation, and the corresponding quadratic behavior around the $k = \pi/2$ minimum. Yet, the gap is overestimated by the variational approach (cyan line) but the shape of the curve is well reproduced. Using the variational approach and assuming three independent spinons, one obtains the lowest part of the $S^z_{\text{tot}} = 3/2$ sector from

$$\omega_{3\text{-spinons}}(k) = \min_{\substack{k_1, k_2, k_3 \\ \sum_i k_i = k}} [\omega(k_1) + \omega(k_2) + \omega(k_3)] , \quad (24)$$

in which $\omega(k)$ is (21) and displayed as the orange curve on Fig. 1 and which can be compared to the boundary of the grey area. Naturally, the three-spinons spectrum is separated from the single spinon branch at low energies because of the gap. Interestingly, for $k \sim \pi/4, 3\pi/4$, the two dispersion relations touch (even cross) each other, telling that the single spinon branch enters the continuum of many spinons. This seems to be in agreement with the ED which shows that the spinon branch separates from the continuum only for $k \in [3\pi/8, 5\pi/8]$. These main features are recovered at the MG point, when $J_2 = 0.5J_1$, with a better agreement between the numerics and the variational approach, as expected. One reaches the incommensurate point for $J_2 = 9/17J_1$ and the ED data display a flattened dispersion relation signaling the onset of incommensurability. The gap is large and separates well the

spinon branch from the three-spinon continuum although the branch clearly enters the continuum on the sides. In the incommensurate regime for $J_2 = 0.6J_1$, the dispersion has a double minimum which shape and position are well reproduced by the variational approach. Yet, the independent spinons picture fails to account for the large gap between the branch and the continuum, which may be due to strong spinon scattering in this regime and the fact that the variational approach becomes less reliable away from the MG point. Last, in the limit of large J_2 , the system is almost equivalent to two decoupled chains, which corresponds to a doubling of the unit cell. Although there is a tiny gap for $J_2 = 4J_1$, the spectrum is again well reproduced by the Bethe ansatz curve which is $J_2 \frac{\pi}{2} |\cos(2k)|$ in this case.

3 Two spinons excitation spectrum

3.1 Variational approach

We now study the elementary excitations on an even length chain at the MG point. They correspond to two-spinons excitations and the natural subspace to describe these excitations is spanned by states of the form $|x_1, x_2\rangle = |\cdots \uparrow \cdots \downarrow \cdots\rangle$ ($x_1 < x_2$) such that the spin sector is determined by the two spinons while the rest of the chain is in the singlet sector because of MG domains. Thanks to spin rotational invariance, we stick to the $S^z_{\text{tot}} = 1$ state for the triplet sector and otherwise to the singlet state. Again, these states constitute a free family that does not span the whole singlet or triplet sectors and they are non-orthogonal. Open boundary conditions are used and the chain is assumed to be infinite in both directions. In this situation, spinons cannot change sublattices so that x_1 remains even and x_2 odd.

3.1.1 Schrödinger equation

As long as spinons do not belong to neighboring sites ($x_1 + 3 \leq x_2$), the effective Hamiltonian will act separately on each spinon, according to (15), and independently of the spin sector

$$(\tilde{\mathcal{H}}_{\text{MG}} - E_{\text{MG}})|x_1, x_2\rangle = \frac{5}{2}J|x_1, x_2\rangle + \frac{J}{2}(|x_1 - 2, x_2\rangle + |x_1 + 2, x_2\rangle + |x_1, x_2 - 2\rangle + |x_1, x_2 + 2\rangle). \quad (25)$$

One then exploits translational invariance by moving to the center of mass frame, introducing variables:

$$X = \frac{x_1 + x_2}{2} \quad \text{and} \quad x = x_2 - x_1, \quad (26)$$

in which x takes odd positives values and X half-integer values. For a given x , all values of X are not allowed. One must have

$$x = 4i \pm 1 \Leftrightarrow X = 2j \pm \frac{1}{2}. \quad (27)$$

Using a Fourier transform on the X coordinate gives states

$$|K, x = 4i \pm 1\rangle = \sum_{X=2j \pm \frac{1}{2}} e^{iKX} |X, x\rangle, \quad (28)$$

in which the first Brillouin zone is $K \in [-\frac{\pi}{2}, \frac{\pi}{2}]$ since the center of mass jumps by two sites for given x . The effective Hamiltonian then takes the following form

$$(\tilde{\mathcal{H}}_{\text{MG}} - E_{\text{MG}})|K, x\rangle = \frac{5}{2}J|K, x\rangle + J \cos K (|K, x - 2\rangle + |K, x + 2\rangle), \quad (29)$$

when $x \geq 3$. The variational wave-function reads

$$|\psi\rangle = \sum_{i \in \mathbb{N}} \int_{-\frac{\pi}{2}}^{\frac{\pi}{2}} \frac{dK}{\pi} \psi_i(K) |K, x = 2i + 1\rangle, \quad (30)$$

which yields to the Schrödinger equation for $i > 1$:

$$(E - E_{\text{MG}}) \psi_i(K) = \frac{5}{2}J \psi_i(K) + J \cos K [\psi_{i-1}(K) + \psi_{i+1}(K)]. \quad (31)$$

3.1.2 Singlet sector

We now have to discuss the case of neighboring spinons which corresponds to the $x = 1$ boundary conditions. There, singlet and triplet sectors behave differently which will be responsible for a bound state.

In the singlet sector, the state $|X, x = 1\rangle$ actually equals the MG state for all X and is an eigenstate of energy E_{MG} . Thus, in the singlet sector, the boundary terms of the Schrödinger equation read

$$(E - E_{\text{MG}}) \psi_1(K) = \frac{5}{2}J \psi_1(K) + J \cos(K) \psi_2(K), \quad (32)$$

$$(E - E_{\text{MG}}) \psi_0(K) = J \cos(K) \psi_1(K). \quad (33)$$

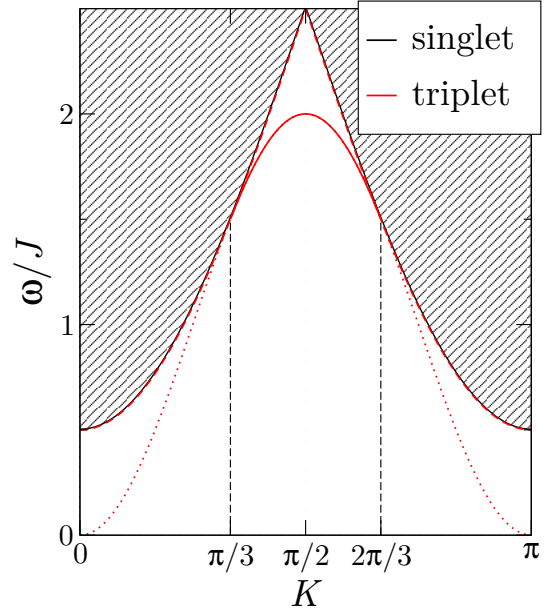


Fig. 2. Low-energy spectrum of the frustrated chain at the MG point. Dashed lines show the continuation of the triplet dispersion relation (42) for which no state exists.

There are two cases: either $\psi_0(K) \neq 0$ or $\psi_0(K) = 0$. If $\psi_0(K) \neq 0$, as $|K, x = 1\rangle$ is already an eigenstate with eigenvalue E_{MG} , the only possible energy is E_{MG} . Then, from (33) we have $\psi_1(K) = 0$ and from (32) we have $\psi_2(K) = 0$. It follows from (31) that $\psi_i(K) = 0$ for $i \neq 0$ and we thus recover $|\text{MG}\rangle$. If $\psi_0(K) = 0$, in which case (32) is equivalent to (31) for $i = 1$ to which one must add the boundary condition

$$\psi_0(K) = 0. \quad (34)$$

Solving (31) with the condition (34) yields plane waves of momentum k as the only possible solutions for the relative motion. Thus a continuum is obtained, displayed on Fig. 2 and which follows

$$\omega(K, k) = \frac{5}{2}J + 2J \cos(K) \cos(2k), \quad (35)$$

where $k \in [-\frac{\pi}{2}, \frac{\pi}{2}]$ and $K \in [-\frac{\pi}{2}, \frac{\pi}{2}]$ (displayed over the range $[0, \pi]$ on Fig. 2).

3.1.3 Triplet sector

In the triplet sector, the action of the effective $\tilde{\mathcal{H}}_{\text{MG}}$ on a contact state $|x, x + 1\rangle$ is

$$(\tilde{\mathcal{H}}_{\text{MG}} - E_{\text{MG}})|x, x + 1\rangle = 3J|x, x + 1\rangle + \frac{J}{2}|x - 2, x - 1\rangle + \frac{J}{2}|x + 2, x + 3\rangle + J|x - 2, x + 1\rangle + J|x, x + 3\rangle, \quad (36)$$

which, once in the center of mass frame and Fourier transformed, gives the equation

$$(\tilde{\mathcal{H}}_{\text{MG}} - E_{\text{MG}})|K, 1\rangle = J(3 + \cos 2K)|K, 1\rangle + 2J \cos K |K, 3\rangle. \quad (37)$$

We then deduce the boundary conditions in the triplet sector

$$(E - E_{\text{MG}})\psi_1(K) = \frac{5}{2}J\psi_1(K) + J\cos(K)\psi_2(K) + 2J\cos(K)\psi_0(K), \quad (38)$$

$$(E - E_{\text{MG}})\psi_0(K) = J(3 + \cos 2K)\psi_0(K) + J\cos(K)\psi_1(K). \quad (39)$$

One last trick is to change variables $\psi_0(K) \rightarrow \psi_0(K)/2$ so that equation (38) gives back Schrödinger's equation (31) with the new boundary condition

$$(E - E_{\text{MG}})\psi_0(K) = J(3 + \cos 2K)\psi_0(K) + 2J\cos(K)\psi_1(K) \quad (40)$$

replacing (39). The boundary condition (40) still possesses plane wave solutions which gives back the continuum of diffusion (35) which is then four times degenerate.

However, the boundary condition (40) now allows to consider bound-state solutions of (31). We then obtain a triplet state (three times degenerate) with the following wave-function

$$\psi_i(K) = \phi(K)e^{-2i/\xi(K)}, \quad (41)$$

in which $\xi(K)$ is the typical width of the spinon bound-state. From (40), the dispersion relation reads

$$\omega(K) = \frac{5}{2}J - J\sqrt{4\cos^2 K + \left(\frac{1}{2} + \cos 2K\right)^2}, \quad (42)$$

for $K \in [\frac{\pi}{3}, \frac{2\pi}{3}]$, so that the bound-state is below the singlet continuum, as illustrated on Fig. 2. Notice that for $K = \pi/2$, the bound-state boils down to $|K = \frac{\pi}{2}, x = 1\rangle$, which is a delocalized triplet shared by two neighboring sites. It can be read directly on (15) that this state is an eigenstate. Last, this calculation provides the behavior of ξ_K as a function of the momentum:

$$e^{-2/\xi(K)} = \frac{\sqrt{4\cos^2 K + \left(\frac{1}{2} + \cos 2K\right)^2} - \frac{1}{2} - \cos 2K}{2\cos K}, \quad (43)$$

which displays a divergence $\xi(K) \rightarrow +\infty$ when $K \rightarrow \frac{\pi}{3}^+$ for which one recovers deconfined excitations as for the singlet sector and the disappearance of the bound-state.

3.2 Evolution of the two-spinon spectrum with increasing frustration

As for the single spinon dispersion relation, we now compare these predictions to numerics from exact diagonalization on Fig. 3. In particular, we show the bottom of the $S_{\text{tot}}^z = 1$ and $S_{\text{tot}}^z = 2$ spectra to discuss the bound state and many-spinons excitations. We could not derive the exact dispersion relation analytically for two spinons away from the MG point, but the single spinon dynamics can already give insights through an independent spinons picture in which the two-spinon dispersion relation reads

$$\omega_{2\text{-spinons}}(K) = \min_{\substack{k_1, k_2 \\ k_1 + k_2 = K}} [\omega(k_1) + \omega(k_2)], \quad (44)$$

in which $\omega(k)$ is (21), and for which singlet and triplet sector are naturally degenerate. Similarly, a four independent spinons dispersion relation can be obtained to compare with numerics.

Starting from the Heisenberg point $J_2 = 0$ the finite-size curve agrees well with the Bethe ansatz lower branch $\omega_{2\text{-spinons}}(K) = J_1 \frac{\pi}{2} \sin K$, and for $J_2 = 0.25J_1$ again with a slightly smaller prefactor and the fact that the tiny gap is not captured on finite-size chains. Notice that in the gapless regime, multi spinons excitations with more than two spinons are as well gapless in the thermodynamical limit which shows up the $S_{\text{tot}}^z = 2$ sector that gets close to the magnon branch.

At the MG point, the dispersion relations for the different spin sectors are very well reproduced by the variational approach. In particular, the triplet bound-state is the lowest $K = \pi/2$ energy. Interestingly, displaying the $S_{\text{tot}}^z = 2$ sector shows that the four spinons continuums start much higher in energy than the two-spinon continuum, essentially because of the single spinon gap, and comes with an increased density of states in the dark grey region. The independent spinons picture shows that close to and at $K = \pi/2$, the lowest boundary of the continuum is actually due to four spinons excitations and not due to two-spinons which lie higher in energies. It also explains why the triplet bound-state hardly detaches from the continuum around $K = \pi/2$, while considering only two-spinon excitations as in Fig. 2 suggested that the bound-state would better separate.

Increasing further the frustration ($J_2 = 9/17J_1$ and $J_2 = 0.6J_1$) brings incommensurability in the dispersion relation. The shapes of the continua are well reproduced by the variational method but, as we saw for a single spinon, the gap is not quantitatively reproduced. Therefore, we shifted the variational curves upward by an amount which is specified on the two plots for each line. The shift for the four spinons line is nearly twice the one for the two spinons line which is reasonable. For $J_2 = 9/17J_1$, the flattening to a quartic behavior for small K is visible in the ED data thanks to the variational curve. The higher part of the spectrum is very similar to the MG point, with the triplet bound-state that still detaches from the continuum by a minute amount. For $J_2 = 0.6J_1$, the incommensurate wave-vector q^* is well resolved by the ED data and in good agreement with the variational prediction. Looking for the minimum over K in (44) gives twice the minimum of the single spinon dispersion relation. Thus, the independent spinon picture gives the following prediction for the incommensurate wave-vector:

$$q^* = \arccos\left(-\frac{5}{4} + \frac{3}{4}\sqrt{2 - \frac{J_1}{J_2}}\right). \quad (45)$$

Interactions between spinons can affect both the magnitude of the gap and the incommensurate wave-vector through their variation with the relative distance. At the MG point, this dependence is very weak at small k since the interaction is essentially local. As the incommensurability in q^* occurs close to the MG point, these corrections should be small. The least one can say is that ED cannot

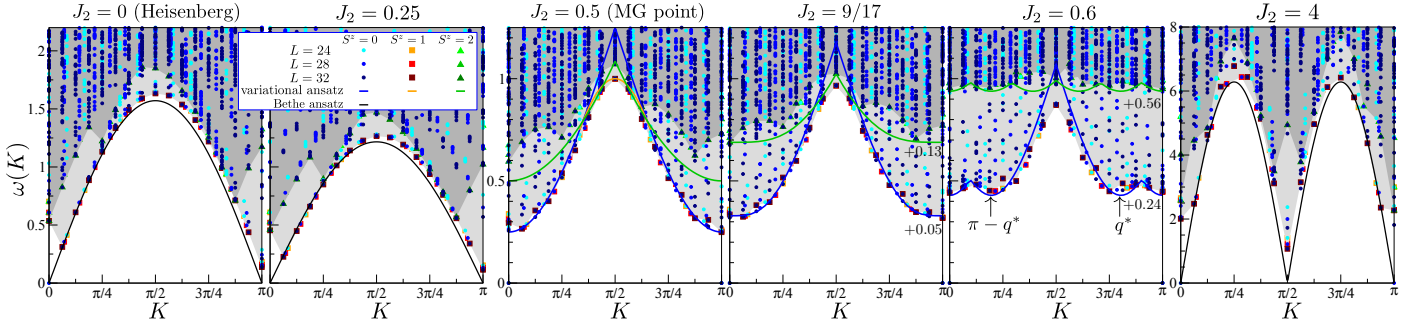


Fig. 3. Two spinons dispersion relations: Evolution of the low-energy spectrum of even size J_1 - J_2 chain for increasing J_2/J_1 , taking $J_1 = 1$ as the unit of energy. The light grey area stands for energy belonging to the $S_{\text{tot}}^z = 1$ sector (2 spinons in a triplet state) while the dark grey area corresponds to the $S_{\text{tot}}^z = 2$ (4 spinons). These are compared to Bethe ansatz (black lines) and the variational approach for two independent spinons (blue line, exact at the MG point) and four independent spinons (green line). The yellow line at the MG point shows the variational result for the triplet bound-state. Extra numbers close to the variational lines for $J_2/J_1 = 9/17, 0.6$ indicate that a vertical shift has been applied to the variational prediction to better fit the ED data.

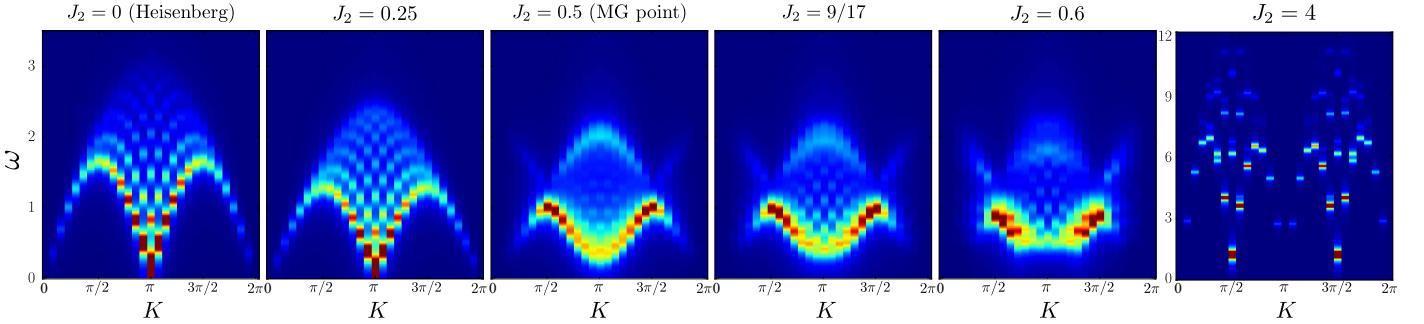


Fig. 4. Dynamical structure factor: Evolution of the dynamical structure factor $\mathcal{S}(K, \omega)$ on an even size J_1 - J_2 chain for the same increasing values of J_2/J_1 as in Fig. 3. Data are obtained from a Lanczos calculation on a $L = 28$ sites chain.

resolve them. Notice that both the ED and the variational ansatz shows that the $K = 0$ energy is actually almost degenerate with the $K = q^*$ energy. This may be seen as a precursor of the degeneracy of the ground-state in the large J_2 limit in which $q^* \rightarrow \pi/2$ gets degenerate with the $K = 0$ sector. Interestingly and as expected from an independent spinon picture, the bottom of the four spinons continuum also displays incommensurability with six minima over the full Brillouin zone.

Last, in the limit of large J_2 and eluding the resolution of the tiny gap of the system, the excitation spectrum is here again well fitted by the Bethe ansatz prediction replacing J_1 by J_2 and folding the first Brillouin zone (see plot for $J_2 = 4J_1$). In Fig. 4, the overall process of gap opening and incommensurate dispersion relation connecting the two limits of a single chain to two chains is illustrated through the experimentally accessible spin dynamical structure factor $\mathcal{S}(K, \omega)$. Lanczos calculations capture a strong redistribution of the spectral weight close to the MG point, with a maximum weight around $K \simeq \pi/2$ and a secondary peak at the higher energies of the two-spinons continuum.

4 Variational approach for the chain with explicit dimerization

In this section, we consider the situation with an explicit dimerization term δ for which the Hamiltonian reads

$$\mathcal{H} = \sum_i (J_1 + (-1)^i \delta) \mathbf{S}_i \cdot \mathbf{S}_{i+1} + J_2 \mathbf{S}_i \cdot \mathbf{S}_{i+2}. \quad (46)$$

Putting ourselves on the Shastry-Sutherland line $\delta + 2J_2 = J_1$ [27], the Hamiltonian is rewritten as

$$\mathcal{H} = \sum_i (2J + \delta) \mathbf{S}_i \cdot \mathbf{S}_{i+1} + J \mathbf{S}_i \cdot \mathbf{S}_{i+2} + (-1)^i \delta \mathbf{S}_i \cdot \mathbf{S}_{i+1}. \quad (47)$$

The ground-state of this Hamiltonian is the MG state with dimers on the strongest bonds $(2i, 2i + 1)$. Its energy is

$$\frac{E_{\text{MG}}}{L} = -\frac{3}{4}(J + \delta). \quad (48)$$

The other MG is no longer an eigenstate and its energy per site remains $-\frac{3}{4}J$ to first order in δ .

4.1 Spinon confinement on a wall

Let us consider an open chain of odd length starting with a weak link $J_1 - \delta$. Due to the lift of the degeneracy, the explicit dimerization generates a confinement of the spinon

close to the boundary through a potential linear with the distance $\propto \delta i$ [38,39]. This effect has been studied analytically in the continuum limit [30,31] and with DMRG [39]. This section provides a proper derivation of the continuum limit based on the RVB basis approach. The explicit dimerization term also generates longer distance hoppings of the spinon, within the variational picture, inducing incommensurability above the Shastry-Sutherland line $\delta > J_1 - 2J_2$. The latter kinetic effect can be neglected when $\delta \ll J$ and the confining potential remains the dominant effect. Within this approximation and choosing a variational wave-function that mimics the $k = \pi/2$ oscillation corresponding to the minimum of the dispersion relation (35)

$$|\psi\rangle = \sum_i (-1)^i \psi_i |2i+1\rangle, \quad (49)$$

the Schrödinger equation for the spinon reads

$$(E - E_{\text{MG}}) \psi_i = \left(\frac{5}{4}J + \frac{3}{2}\delta i \right) \psi_i - \frac{J}{2} (\psi_{i-1} + \psi_{i+1}), \quad (50)$$

to which we add the boundary condition $\psi_{-1} = 0$. This equation can be solved in the continuum limit [31,30], assuming that ψ_i varies slowly enough with i . In the continuum limit, one has

$$-2J\psi''(x) + \frac{3\delta}{4}(x - \varepsilon)\psi(x) = 0, \quad (51)$$

in which $\psi(x = 2i+1) = \psi_i$ and $\varepsilon = \frac{4}{3\delta}(E - E_{\text{MG}}) - \frac{J}{3\delta}$, that is equivalent to

$$\psi''(y) - y\psi(y) = 0, \quad (52)$$

after changing variables as follows

$$y = \frac{1}{\xi_{\text{conf}}} (x - \varepsilon), \quad \text{with} \quad \xi_{\text{conf}} = \left(\frac{8J}{3\delta} \right)^{1/3}. \quad (53)$$

ξ_{conf} is the typical confinement length. In the limit of small $\delta \ll J$, one gets $\xi_{\text{conf}} \gg 1$, so that taking the continuum limit is justified. A natural set of solutions for the differential equation (52) are Airy functions Ai and Bi that oscillate for $x < 0$ and with asymptotic behaviors

$$\text{Ai}(x) \xrightarrow{x \rightarrow +\infty} 0, \quad \text{Bi}(x) \xrightarrow{x \rightarrow +\infty} +\infty. \quad (54)$$

The boundary conditions $\psi(x = -1) = 0$ and $\psi(x) \xrightarrow{x \rightarrow +\infty} 0$ allow the following energies

$$E_n = E_{\text{MG}} + \frac{J}{4} - \frac{3\delta}{4}(1 + a_n \xi_{\text{conf}}), \quad (55)$$

in which the $a_n < 0$ are zeros of the Ai function. The associated wave-functions read

$$\psi_n(x) \propto \text{Ai} \left(\frac{x+1}{\xi_{\text{conf}}} + a_n \right). \quad (56)$$

These states and their energy are represented on Fig. 5. Exact magnetization profiles obtained from DMRG have been compared to such analysis in Refs. [31] and [50].

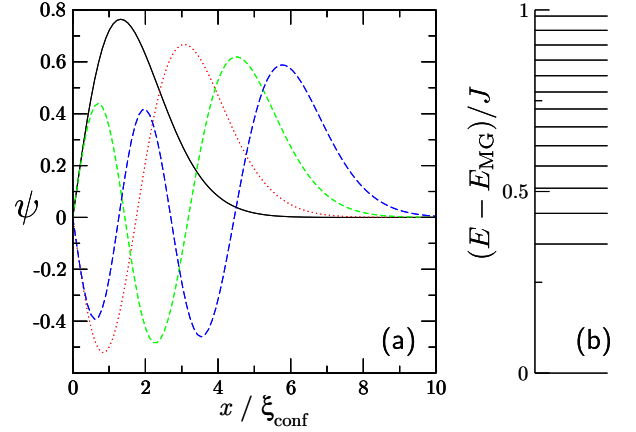


Fig. 5. (a) Airy functions corresponding to the first excited states confined close to $x = 0$. (b) Corresponding energy levels for $\delta = 0.01J$.

4.2 Two spinons excitations

In the case of an even chain with infinite number of sites and containing two spinons, the explicit dimerization term yields a linear (or string) attractive potential between the two domain walls. Writing Schrödinger equation in the center of mass frame and taking the continuum limit leads to

$$-4J \cos(K) \partial_x^2 \psi(K, x) + \frac{3\delta}{4} [x - \varepsilon(K)] \psi(K, x) = 0, \quad (57)$$

where

$$\varepsilon(K) = \frac{4}{3\delta} (E - E_{\text{MG}}) - \frac{2J}{3\delta} (5 - 4 \cos K). \quad (58)$$

Using the change of variables

$$y = \frac{x - \varepsilon(K)}{\xi_{\text{conf}}(K)}, \quad \text{with} \quad \xi_{\text{conf}}(K) = \left(\frac{16J}{3\delta} \cos K \right)^{1/3}, \quad (59)$$

one recovers (52). When $K \rightarrow \pi/2$, $\xi_{\text{conf}} \rightarrow 0$ and taking the continuum limit is no longer justified. However, for $K = \pi/2$, Schrödinger equation simply reads

$$(E - E_{\text{MG}}) \psi_i = \left(\frac{5}{2}J + \frac{3}{2}\delta i \right) \psi_i. \quad (60)$$

So the eigenstates are simply states with spinons at constant relative distances $x = 2i + 1$. The corresponding energies are given by

$$\omega_i(\pi/2) = \frac{5}{2}J + \frac{3}{2}\delta i, \quad (i > 0). \quad (61)$$

In the triplet sector, the bound-state with $i = 0$ is still there, which energy $\omega_0(\pi/2) \simeq 2J$ is given by the boundary condition (40). For $K < \pi/2$, the eigenstates are shifted Airy functions

$$\psi(K, x) \propto \text{Ai} \left(\frac{x - \varepsilon(K)}{\xi_{\text{conf}}(K)} \right), \quad (62)$$

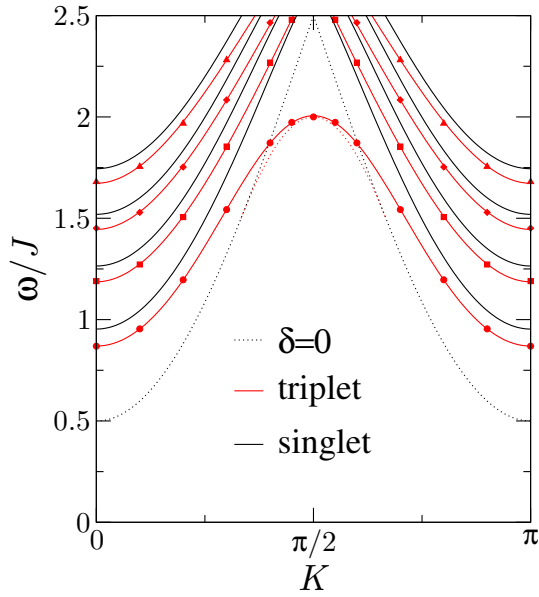


Fig. 6. Low-energy spectrum of the MG chain with explicit dimerization $\delta = 0.05J$, as computed from RVB variational calculations in the continuum limit. In the triplet sector, symbols stand for numerical solutions of (64) and thick lines are guide to the eyes.

meaning that these are bound-states with characteristic length $\xi_{\text{conf}}(K)$. Energies are determined from boundary conditions (34) in the singlet sector, and (40) in the triplet sector. The singlet sector directly gives the dispersion relation as a function of the zeros a_n of the Airy function Ai :

$$\omega_n(K) = J \left(\frac{5}{2} - 2 \cos K \right) + \frac{3\delta}{4} [1 - a_n \xi_{\text{conf}}(K)] . \quad (63)$$

In the triplet sector, the implicit equation on the energy E can be rewritten as

$$-2 \cos(K) \text{Ai} \left(\frac{3 - \varepsilon(K)}{\xi_{\text{conf}}(K)} \right) = \left(\frac{3}{4} \frac{\delta}{J} \varepsilon(K) - \left(\frac{1}{2} + 2 \cos K + \cos 2K \right) \right) \text{Ai} \left(\frac{1 - \varepsilon(K)}{\xi_{\text{conf}}(K)} \right), \quad (64)$$

which we solve numerically to obtain the spectra $E_n(K)$ and the corresponding dispersion relations $\omega_n(K)$. On Fig. 6, the first triplet and singlet dispersion relations are displayed. The lowest part of the continuum (35) now divides into single triplet and singlet branches. These formation of bound-states can be also studied from a weakly coupled dimer picture ($J_1 - \delta \ll J_1$) followed by series expansion of the coupling [44]. The behavior is consistent with numerical studies of the elementary excitations of this model [39, 40, 42, 51].

5 Conclusion

We obtained effective Schrödinger equations for the motion of a single or two spinons in the frustrated chain by

using the inverse of the overlap matrix of the short-range RVB basis. In some peculiar cases, the equations can be solved analytically, recovering known results and providing new ones on the excitation spectra. ED results are well accounted for, even for four-spinons continuum, assuming an independent spinon picture. This approach is somewhat systematic as it does not depend on the Hamiltonian, yet it works better when the low-energy physics is well captured by dimer states. For instance, it gave quantitative predictions in the random MG model [48].

Frustrated chains are still an active field of experimental research [52, 53, 54] and this approach could shed light on related models. Furthermore, it would be interesting to seek generalizations of the MG physics to higher spins, as proposed in [55, 56, 57] and to see whether such approach could be also generalized. In particular, the case of spin 3/2 which is now relevant experimentally [58, 59] displays a qualitatively similar phase diagram [60] as spin-1/2, yet with the possibility to stabilize chiral phases in the presence of anisotropy [61, 62]. Such model would constitute a first step towards a generalization.

Acknowledgements

We thank Matthieu Mambrini for insightful discussions. We acknowledge support from the French ANR program ANR-2011-BS04-012-01 QuDec.

References

1. P. Lecheminant, *Frustrated Spin Systems*, chap. One-Dimensional Quantum Spin Liquids, p. 307, (World Scientific, 2004), cond-mat/0306520.
2. F. D. M. Haldane, Phys. Rev. B **25**, 4925 (1982).
3. T. Tonegawa and I. Harada, J. Phys. Soc. Jpn. **56**, 2153 (1987).
4. V. J. Emery and C. Noguera, Phys. Rev. Lett. **60**, 631 (1988).
5. K. Okamoto and K. Nomura, Physics Letters A **169**, 433437 (1992).
6. S. Eggert, Phys. Rev. B **54**, R9612 (1996).
7. S. R. White and I. Affleck, Phys. Rev. B **54**, 9862 (1996).
8. C. Majumdar and D. Ghosh, J. Math. Phys. **10**, 1388 (1969).
9. C. Majumdar and D. Ghosh, J. Math. Phys. **10**, 1399 (1969).
10. J. Villain, J. Phys. Chem. Solids **11**, 303 (1959).
11. A. A. Aligia, C. D. Batista, and F. H. L. Eßler, Phys. Rev. B **62**, 3259 (2000).
12. M. Kumar, Z. G. Soos, D. Sen, and S. Ramasesha, Phys. Rev. B **81**, 104406 (2010).
13. K. Nomura, J. Phys. Soc. Jpn. **72**, 476 (2003).
14. C. Zeng and J. B. Parkinson, Phys. Rev. B **51**, 11609 (1995).
15. D. Arovas and S. Girvin, *Recent Progress in Many-Body Theories*, chap. Exact Questions to Some Interesting Answers in Many Body Physics, pp. 315–344, (Springer US, 1992).

16. R. Bursill, G. A. Gehring, D. J. J. Farnell, J. B. Parkinson, T. Xiang, and C. Zeng, *J. Phys.: Condens. Matter* **7**, 8605 (1995).
17. D. P. Arovas, A. Auerbach, and F. D. M. Haldane, *Phys. Rev. Lett.* **60**, 531 (1988).
18. U. Schollwöck, T. Jolicœur, and T. Garel, *Phys. Rev. B* **53**, 3304 (1996).
19. O. Golinelli, T. Jolicœur, and E. Sørensen, *Eur. Phys. J. B* **11**, 199 (1999).
20. A. Lavarélo, G. Roux, and N. Laflorencie, *Phys. Rev. B* **84**, 144407 (2011).
21. J. des Cloizeaux and J. J. Pearson, *Phys. Rev.* **128**, 2131 (1962).
22. T. Yamada, *Prog. Theor. Phys.* **41**, 880 (1969).
23. K. Hashimoto, *Prog. Theor. Phys.* **68**, 1122 (1982).
24. T. Barnes, *Phys. Rev. B* **67**, 024412 (2003).
25. J.-S. Caux and R. Hagemans, *J. Stat. Mech.* **2006**, P12013 (2006).
26. M. Mourigal, M. Enderle, A. Klöpperpieper, J.-S. Caux, A. Stunault, and H. M. Rønnow, *Nature Physics* **9**, 435 (2013).
27. B. S. Shastry and B. Sutherland, *Phys. Rev. Lett.* **47**, 964 (1981).
28. W. J. Caspers, K. M. Emmett, and W. Magnus, *J. Phys. A: Math. Gen.* **17**, 2687 (1984).
29. H. Frahm and J. Schliemann, *Phys. Rev. B* **56**, 5359 (1997).
30. T. M. R. Byrnes, M. T. Murphy, and O. P. Sushkov, *Phys. Rev. B* **60**, 4057 (1999).
31. G. S. Uhrig, F. Schoenfeld, M. Laukamp, and E. Dagotto, *Eur. Phys. J. B* **7**, 67 (1999).
32. V. V. Mkhitarian and T. A. Sedrakyan, *Ann. Henri Poincaré* **7**, 1579 (2006).
33. J. Kokalj and P. Prelovšek, *Phys. Rev. B* **82**, 060406 (2010).
34. A. Deschner and E. S. Sørensen, *J. Stat. Mech.* **2011**, P10023 (2011).
35. A. Deschner and E. S. Sørensen, *Phys. Rev. B* **87**, 094415 (2013).
36. S. Brehmer, A. K. Kolezhuk, H.-J. Mikeska, and U. Neugebauer, *J. Phys.: Condens. Matter* **10**, 1103 (1998).
37. R. Chitra, S. Pati, H. R. Krishnamurthy, D. Sen, and S. Ramasesha, *Phys. Rev. B* **52**, 6581 (1995).
38. I. Affleck, in *Dynamical Properties of Unconventional Magnetic Systems*, NATO Advanced Study Institute, Series E: Applied Sciences, edited by A. Skjeltrop and D. Sherrington (Kluwer Academic, Dordrecht, 1998), Vol. **349**, pp. 123-131, See also arXiv:cond-mat/9705127.
39. E. Sørensen, I. Affleck, D. Augier, and D. Poilblanc, *Phys. Rev. B* **58**, R14701 (1998).
40. G. Bouzerar, A. P. Kampf, and G. I. Japaridze, *Phys. Rev. B* **58**, 3117 (1998).
41. D. Augier, E. Sørensen, J. Riera, and D. Poilblanc, *Phys. Rev. B* **60**, 1075 (1999).
42. P. V. Shevchenko, V. N. Kotov, and O. P. Sushkov, *Phys. Rev. B* **60**, 3305 (1999).
43. T. Barnes, J. Riera, and D. A. Tennant, *Phys. Rev. B* **59**, 11384 (1999).
44. W. Zheng, C. J. Hamer, R. R. P. Singh, S. Trebst, and H. Monien, *Phys. Rev. B* **63**, 144410 (2001).
45. C. J. Hamer, W. Zheng, and R. R. P. Singh, *Phys. Rev. B* **68**, 214408 (2003).
46. K. P. Schmidt, C. Knetter, and G. S. Uhrig, *Phys. Rev. B* **69**, 104417 (2004).
47. S. Takayoshi and M. Oshikawa, *Phys. Rev. B* **86**, 144408 (2012).
48. A. Lavarélo and G. Roux, *Phys. Rev. Lett.* **110**, 087204 (2013).
49. R. Saito, *J. Phys. Soc. Jpn.* **59**, 482 (1990).
50. R. L. Doretto and M. Vojta, *Phys. Rev. B* **80**, 024411 (2009).
51. R. R. P. Singh and Z. Weihong, *Phys. Rev. B* **59**, 9911 (1999).
52. B. Gibson, R. Kremer, A. Prokofiev, W. Assmus, and G. McIntyre, *Physica B: Condensed Matter* **350**, E253 (2004), Proceedings of the Third European Conference on Neutron Scattering.
53. M. Schäpers, A. U. B. Wolter, S.-L. Drechsler, S. Nishimoto, K.-H. Müller, M. Abdel-Hafiez, W. Schottenhamel, B. Büchner, J. Richter, B. Ouladdiaf, M. Uhlarz, R. Beyer, Y. Skourski, J. Wosnitza, K. C. Rule, H. Ryll, B. Klemke, K. Kiefer, M. Reehuis, B. Willenberg, and S. Süllow, *Phys. Rev. B* **88**, 184410 (2013).
54. M. B. Stone, Y. Chen, D. H. Reich, C. Broholm, G. Xu, J. R. D. Copley, and J. C. Cook, *ArXiv e-prints*, 1406.7596.
55. S. Rachel, *Europhys. Lett.* **86**, 37005 (2009).
56. F. Michaud, F. Vernay, S. R. Manmana, and F. Mila, *Phys. Rev. Lett.* **108**, 127202 (2012).
57. J. M. Matera and C. A. Lamas, *ArXiv e-prints*, 1403.3737.
58. F. Damay, C. Martin, V. Hardy, A. Maignan, G. André, K. Knight, S. R. Giblin, and L. C. Chapon, *Phys. Rev. B* **81**, 214405 (2010).
59. F. Damay, C. Martin, V. Hardy, A. Maignan, C. Stock, and S. Petit, *Phys. Rev. B* **84**, 020402 (2011).
60. R. Roth and U. Schollwöck, *Phys. Rev. B* **58**, 9264 (1998).
61. P. Lecheminant, T. Jolicœur, and P. Azaria, *Phys. Rev. B* **63**, 174426 (2001).
62. T. Hikihara, M. Kaburagi, and H. Kawamura, *Phys. Rev. B* **63**, 174430 (2001).